Transverse chromatic aberration across the visual field of the human eye

Simon Winter

Department of Applied Physics,
Biomedical and X-Ray Physics,
KTH Royal Institute of Technology, Stockholm, Sweden

Ramkumar Sabesan

Department of Ophthalmology,
University of Washington, Seattle, WA, USA

Pavan Tiruveedhula

School of Optometry, University of California,
Berkeley, CA, USA

Claudio Privitera

School of Optometry, University of California,
Berkeley, CA, USA

Peter Unsbo

Department of Applied Physics,
Biomedical and X-Ray Physics,
KTH Royal Institute of Technology, Stockholm, Sweden

Linda Lundström

Department of Applied Physics,
Biomedical and X-Ray Physics,
KTH Royal Institute of Technology, Stockholm, Sweden

Austin Roorda

School of Optometry, University of California,
Berkeley, CA, USA
Vision Science Graduate Group, University of California,
Berkeley, CA, USA

The purpose of this study was to measure the transverse chromatic aberration (TCA) across the visual field of the human eye objectively. TCA was measured at horizontal and vertical field angles out to $\pm15°$ from foveal fixation in the right eye of four subjects. Interleaved retinal images were taken at wavelengths 543 nm and 842 nm in an adaptive optics scanning laser ophthalmoscope (AOSLO). To obtain true measures of the human eye's TCA, the contributions of the AOSLO system's TCA were measured using an on-axis aligned model eye and subtracted from the ocular data. The increase in TCA was found to be linear with eccentricity, with an average slope of 0.21 arcmin/degree of visual field angle (corresponding to 0.41 arcmin/degree for 430 nm to 770 nm). The absolute magnitude of ocular TCA varied between subjects, but was similar to the resolution acuity at 10° in the nasal visual field, encompassing three to four cones. Therefore, TCA can be visually significant. Furthermore, for high-resolution imaging applications, whether visualizing or stimulating cellular features in the retina, it is important to consider the lateral displacements between wavelengths and the variation in blur over the visual field.

Introduction

The optical errors of the human eye are often only corrected for central vision within a limited spectral range. However, good optical quality over larger viewing angles and over a wider spectrum is important for many applications in optometry and ophthalmology, such as peripheral vision and retinal imaging. Monochromatic refractive corrections are known to enhance image quality, but further improvements require knowledge about the chromatic aberration of

the eye. In particular, little is known about the peripheral transverse chromatic aberration. This study presents the first objective measurements of the transverse chromatic aberration over the visual field of the human eye.

The optics of the human eye generally provides the best image quality for objects that are located close to its optical axis. Optical errors such as off-axis astigmatism and coma increase rapidly when the object is moved out in the peripheral visual field. Furthermore, light undergoes dispersion in the ocular media, which has a refractive index profile similar to water. This dispersion manifests itself as chromatic aberration (CA) and causes rays of different wavelengths to follow different paths in the eye, reaching different locations on the retina. The CA of the eye is usually divided into two kinds: longitudinal, or axial, chromatic aberration (LCA) and transverse, or lateral, chromatic aberration (TCA). The first one, LCA, renders the eye to be relatively more myopic (or less hyperopic) for shorter (blue) than for longer (red) wavelengths. LCA has been found to be relatively constant over the field of view (Jaeken, Lundström, & Artal, 2011; Rynders, Navarro, & Losada, 1998). In contrast, TCA is defined as the angular offset between the chief rays of different wavelengths and increases with the angle of the light relative to the best optical axis (Thibos, 1987). This angular offset results in different retinal image positions for point sources and in different magnifications for extended objects depending on wavelength (Atchison & Smith, 2000). Consequently, chromatic errors will reduce the contrast of the polychromatic retinal image, and the reduction will generally increase with eccentricity in the peripheral field.

There are many applications that would benefit from a better image quality over a large visual field. Correcting the peripheral optical errors can, for example, improve vision for people with central visual field loss (Baskaran, Rosén, Lewis, Unsbo, & Gustafsson, 2012; Gustafsson & Unsbo, 2003; Lundström, Gustafsson, & Unsbo, 2007). Correction of peripheral optical errors can also enhance the resolution and contrast in retinal imaging, e.g., when imaging rods (Dubra et al., 2011). Furthermore, the peripheral image quality may influence the process of emmetropization (see Holden et al., 2014, for a recent review). The studies mentioned already have mainly concentrated on the monochromatic optical errors, and less attention has been paid to the eye's CA. The simple use of monochromatic light to eliminate effects of CA is not a practical option for many situations. For example, functional vision is inherently polychromatic and the techniques of broadband, multispectral, and fluorescence imaging all rely on polychromatic light. To develop more useful approaches to compensate for CA, the magnitude of CA first needs to be known.

Quantifications of the ocular CA over the visual field are rare. To our knowledge, only two studies on peripheral LCA and three on peripheral TCA have previously been presented. Because LCA is relatively constant over the population (Vinas, Dorronsoro, Cortes, Pascual, & Marcos, 2015) as well as over the field of view (Jaeken et al., 2011; Rynders et al., 1998), a population estimation of the foveal LCA is generally sufficient for predicting the peripheral LCA. Conversely, foveal TCA varies over the population (Marcos, Burns, Moreno-Barriusop, & Navarro, 1999; Ogboso & Bedell, 1987; Rynders, Lidkea, Chisholm, & Thibos, 1995; Simonet & Campbell, 1990) and the theoretical article by Thibos suggests that TCA changes nearly linearly with eccentric viewing angle (Thibos, 1987). The two experimental studies on peripheral TCA indeed confirm that TCA changes with viewing angle. In the first study, Ogboso and Bedell used a subjective alignment method and found the TCA to increase with eccentricity (Ogboso & Bedell, 1987). In the second study, Winter et al. (2015) evaluated the effect of prism-induced TCA on foveal and peripheral vision and found that different prisms were needed to optimize peripheral vision compared with central vision. The reason for the low number of studies on peripheral TCA is due to the difficulties in estimating its magnitude by adequate measurement procedures. The two subjective studies of peripheral TCA mentioned already showed large variations and were very time-consuming. To be able to compensate for the ocular TCA, we therefore need robust, objective methods to measure its magnitude across the visual field. A simple double-pass approach will cancel out the TCA that is induced when light enters the eye because the light reflected back from the retina will experience the reverse TCA on its propagation out of the eye.

In this study we have implemented an objective technique to quantify the ocular TCA over the visual field. The technique utilizes the lateral offsets in high-resolution retinal images taken simultaneously with different wavelengths in an adaptive optics scanning laser ophthalmoscopy (AOSLO) system as previously described (Grieve, Tiruveedhula, Zhang, & Roorda, 2006; Harmening, Tiruveedhula, Roorda, & Sinnich, 2012). The offsets, after using a model eye to correct for TCA inherent in the imaging system itself, can measure ocular TCA quickly and accurately across the visual field. This article explains the methodology and presents objective measurements of the magnitude of ocular TCA over the central 30° field of four subjects.

Methods

All measurements were performed with an AOSLO system (Roorda et al., 2002) with a MEMS deformable mirror (model Multi-3.5, 140 actuators, 3.5 μm stroke, Boston Micromachines Corp., Cambridge, MA). In short, the AOSLO produces high-resolution videos of the retinal structures in the living human eye by scanning a focused beam of light over the retina and recording the back-reflected light. High resolution and contrast is achieved by a confocal design and by correcting the optical errors of the eye with a deformable mirror and a wavefront sensor working in closed-loop. In this study, the imaging was performed in infrared (IR) light (842 ± 25 nm) over a retinal area of 1.35° (512 × 512 pixels). Simultaneously, green light (543 ± 11 nm) was used to image a smaller 0.34° × 0.68° region of the retina (126 × 256 pixels) spatially interleaved, line-by-line, with the IR light. The green and the IR channels were detected separately by dedicated photomultiplier tubes and combined into a single imaging channel in the AOSLO. The population average of LCA was compensated for by adjusting the relative vergence at the two wavelengths (see equation 5a in Atchison & Smith, 2005). Furthermore, the defocus setting of the adaptive mirror was set to balance any remaining small differences between wavelengths to make the photoreceptor structure visible for both green and IR simultaneously (Grieve et al., 2006). To estimate the TCA, the specific method described by Harmening et al. (2012) was used. The total TCA was estimated through 2D cross-correlation of the images simultaneously collected at the two wavelengths. This total TCA contains contributions from the eye as well as from the AOSLO system. The contribution from the AOSLO originates from a slight lateral displacement between the green and the IR beam in the AOSLO system, and is here denoted "system TCA." We therefore also implemented an artificial model eye that had similar LCA as the human eye, but was free from on-axis TCA. As described in more detail as follows, this model eye was used to measure the TCA of the AOSLO system alone. By subtracting this system TCA from the measured total TCA, we could extract the ocular TCA.

Measuring system TCA

The artificial model eye consisted of an iris diaphragm, a plano-convex lens (Glass N-SF5 with radius 16.82 mm, $n_d = 1.673$, and $V_d = 32.30$), and an "image plane" (end cap plug with a center pit). The elements were mounted in air in a lens tube and the length was adjusted to render close to emmetropia

when measured through the AOSLO. The LCA of the model eye was 1.25 D compared with the Chromatic Eye of 1.22 D between 543 nm and 842 nm (Thibos, Ye, Zhang, & Bradley, 1992). A precise alignment of the model eye was crucial to correctly measure the contributions of the AOSLO system TCA, because the model eye will introduce additional TCA if its axis is not aligned with the optical axis of the AOSLO. A pupil camera was therefore mounted in an oblique angle and focused on the exit pupil of the AOSLO as a reference to control the position of the model eye (see Figure 1). Additionally, centration was fine-tuned by adjusting the tip and tilt of the model eye to minimize the astigmatism measured by the AOSLO at the same time as the center pit of the model eye retina was centered in the image field. The system TCA was then measured by recording interleaved videos of the model eye. The cross-correlation returned the x–y pixel locations for the green light, with the IR location as the reference. To ensure correct measures of the system TCA, these measurements were repeated on each measurement day.

Measuring ocular TCA

Four emmetropic subjects between 27 and 31 years old and with good ocular health participated in the study. All subjects were familiar with the testing procedure and gave written informed consent before participating in the study. The University of California Institutional Review Board approved the research and the experimental procedures conformed to the Declaration of Helsinki. The measurements were performed in the right eye (the left eye was occluded) of the four subjects at different field angles in the nasal, temporal, superior, and inferior visual field from 0.5° out to a maximum of 15° from foveal fixation (for subject S4, only the horizontal meridian was measured). For all subjects, the pupil was dilated and cyclopleged (use of tropicamide 1% solution, and, if necessary, additional phenylephrine hydrochloride 2.5% solution; reapplication as needed depending on pupil size). Furthermore, artificial tears were sometimes used to support the tear film.

For the measurements of ocular TCA, the human eye was aligned similar to the model eye, but the subject was looking at the fixation targets via the beamsplitter (see Figure 1). The beam was centered on the eye's pupil, and the eye's pupil was aligned to the exit pupil of the system in X–Y–Z direction using the pupil camera. The monochromatic optical errors were corrected in closed loop by the deformable mirror of the AOSLO (no trial lenses). As for the model eye, interleaved retinal videos of the subjects' eyes were recorded (90 frames in 3 s) and analyzed by two-
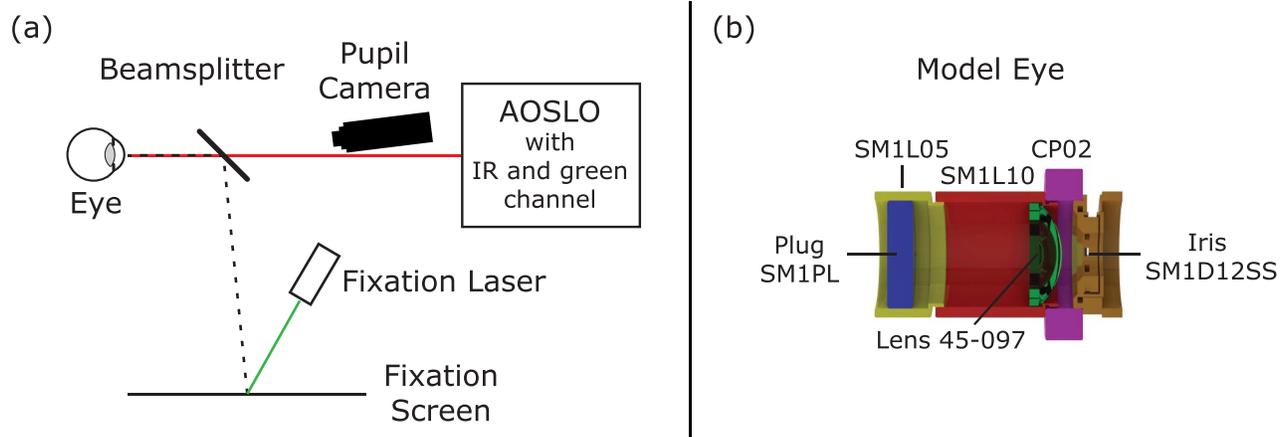
Figure 1. (a) Setup for objective measurements of TCA over the visual field (schematic illustration seen from above). The position of the eye was monitored by a pupil camera and the subject looked at an illuminated fixation target 1 meter away via a beamsplitter. (b) To determine the AOSLO system's TCA the subject's eye was replaced with the artificial model eye (here all part numbers given are from Thorlabs, except for the lens, which is from Edmund Optics).

dimensional cross-correlation. It was attempted to measure at angles of 0.5°, 2.5°, 5°, 7.5°, 10°, 12.5°, and 15° from fixation in all four visual field directions, but that was not possible in all meridians and on all subjects. All measurements included at least two sequential videos at each possible measurement angle. Moreover, each measurement angle was measured with at least two repetitions with a completely new realignment of the subject's eye in between.

Measuring cone spacing

The measurement of TCA involved recording images of the photoreceptor mosaic at each location, providing the opportunity to measure photoreceptor spacing at any tested location. Using a method described previously by Duncan et al. (2007), cone spacing was measured at 10° in the four field directions from two videos in each direction for each subject (Duncan et al., 2007).

Results

The ocular TCA between 543 nm and 842 nm for four emmetropic subjects over the horizontal and the vertical meridian is presented in Figures 2 and 3. The values are corrected for the AOSLO system's TCA as measured with the model eye. The system's TCA had a total magnitude of around 4.6 arcmin, with approximately equal components along the horizontal and vertical directions, which shows the importance of correcting for this factor. The measurements of the system's TCA were very repeatable; the standard

deviation between repeated tests on different days (provided no realignment of the AOSLO system was performed) was 0.18 arcmin and the maximum difference was 0.5 arcmin. It is worth noting that the different repetitions of ocular TCA measurements on subject S2 over the horizontal field were performed on several occasions, with realignment of the AOSLO system in between, but still showed consistent results (see Figure 2).

A two-way analysis of variance showed that the ocular TCA data in Figures 2 and 3 varied significantly both with eccentricity and in-between subjects ($p < 0.05$). Furthermore, there was a significant interaction between the main effects eccentricity and subject indicating that the rate of change in TCA with eccentricity varied between subjects. The data points in the figures were fitted by a linear regression, where the slope reveals the rate of change in the TCA (in arcmin) with eccentricity (in degrees) and the constant represents the foveal TCA (in arcmin), both given in Table 1. TCA was found to increase linearly with off-axis angle; the average rate was 0.19 arcmin/degree in the horizontal meridian and 0.23 arcmin/degree in the vertical meridian. Taking the average over both meridians results in an average rate of 0.21 arcmin/ degree. For some of the subjects it was not possible to obtain TCA data for all fixation angles because of insufficient image quality for the 2D cross-correlation.

The TCA values in the different visual field directions in Table 2 were calculated from the fitted linear functions of Table 1. The absolute magnitude of peripheral TCA between green and IR varied to some extent between subjects, reflecting the intersubject variation in the magnitude of foveal TCA: In the horizontal meridian from 1.8 to 2.5 arcmin, and in the vertical meridian from 0.0 to 1.1 arcmin. At 10°
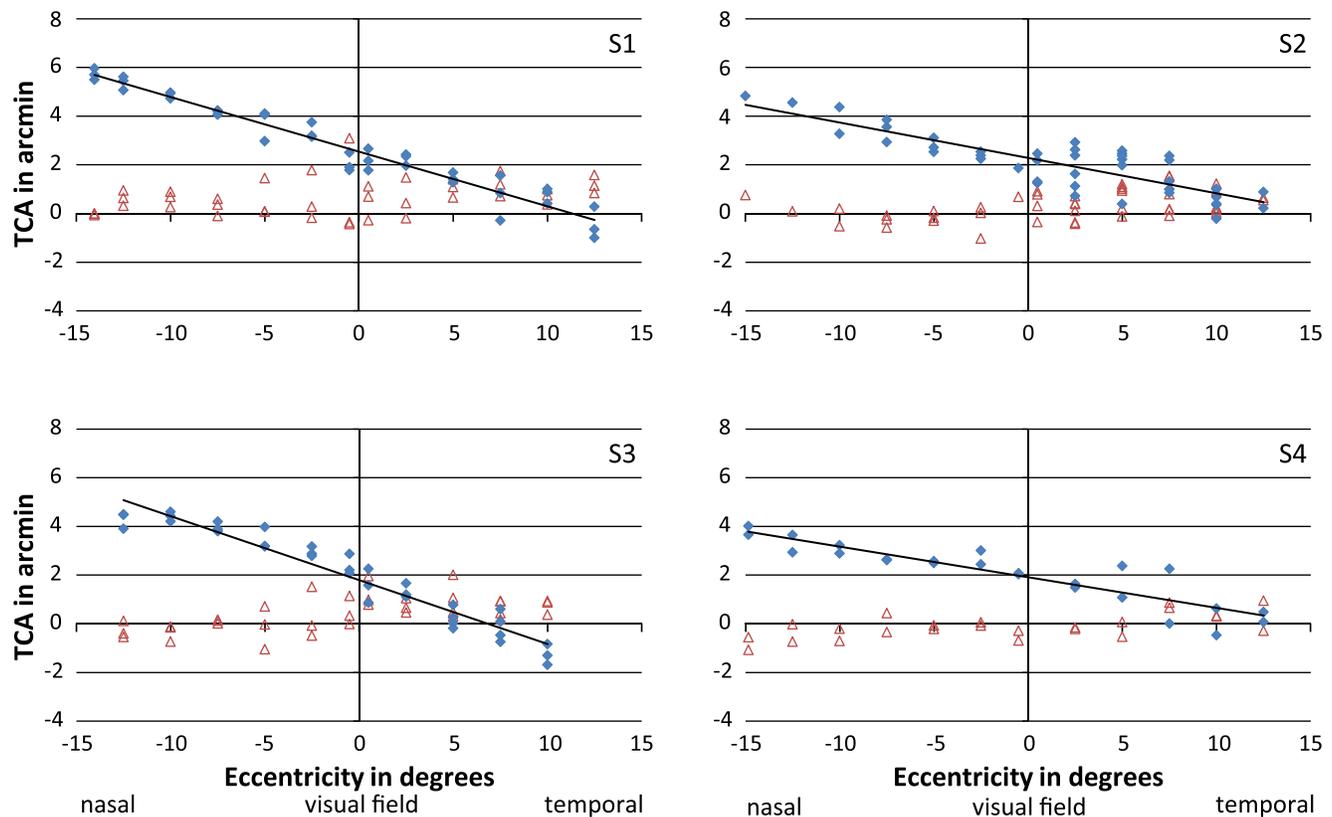
Figure 2. TCA in the horizontal meridian for four subjects S1–S4. The blue diamonds show the horizontal TCA, the red hollow triangles the vertical TCA, and the line is a linear regression with the data given in Table 1. A positive sign of horizontal TCA means that the direction of TCA is the same as a base-in prism would cause (i.e., short wavelengths will end up at the retina more toward the nasal retina than the longer wavelengths). In the same manner a positive sign for vertical TCA corresponds with a base-up prism.

eccentricity, the highest magnitude of TCA occurred in the nasal visual field and was between 3.2 and 4.8 arcmin (the 10° temporal visual field is closer to the achromatic axis of the eye). Table 2 also includes cone photoreceptor spacing at 10° for the four different field directions. For comparison, the last column of the table gives the estimate of the midget ganglion cell receptive field sizes at the same locations using the formula of Watson (2014).

Discussion

To summarize, this study presents the first objective measurements of the TCA of the human eye across the central 30° visual field. The results show that TCA changes linearly over this visual field with a rate of approximately 0.21 arcmin/degree in the four studied subjects for wavelengths of 543 and 842 nm.

In this study the range of measured angles was restricted to 0.5° to 15° eccentricity due to limitations in detecting the cones in the retinal image. In the fovea, cones were not easily distinguishable due to their small size. In the periphery outside the central 30°, the

dynamic range of the deformable mirror was insufficient to compensate for off-axis aberrations. This insufficient image texture led to erroneous cross-correlation values, especially around the optic disk and such cases were discarded.

The main source of the measurement variation in the ocular TCA (shown in Figures 2 and 3) was the centration of the pupil relative to the measurement axis of the AOSLO. In the presence of an artificial pupil, the induced TCA (in milliradians) can be approximated by the product of the LCA (in diopters) and the displacement of the aperture from the visual axis (in millimeters; Thibos, Bradley, Still, Zhang, & Howarth, 1990). Applying this approximation to an LCA of 1.22 D, as estimated with the Chromatic Eye model for the applied wavelengths (Thibos et al., 1992), an aperture displacement of 1 mm would then cause a shift in TCA of about 4.2 arcmin. In a recent study on the same AOSLO system, the shift in TCA due to pupil decentration was experimentally measured to be 3.5 arcmin/mm (Privitera, Sabesan, Winter, Tiruveed-hula, & Roorda, 2016). Consequently, small fluctuations in the alignment of the subjects' pupil or of the model eye can cause substantial changes in the measured TCA. Such random fluctuations in the TCA
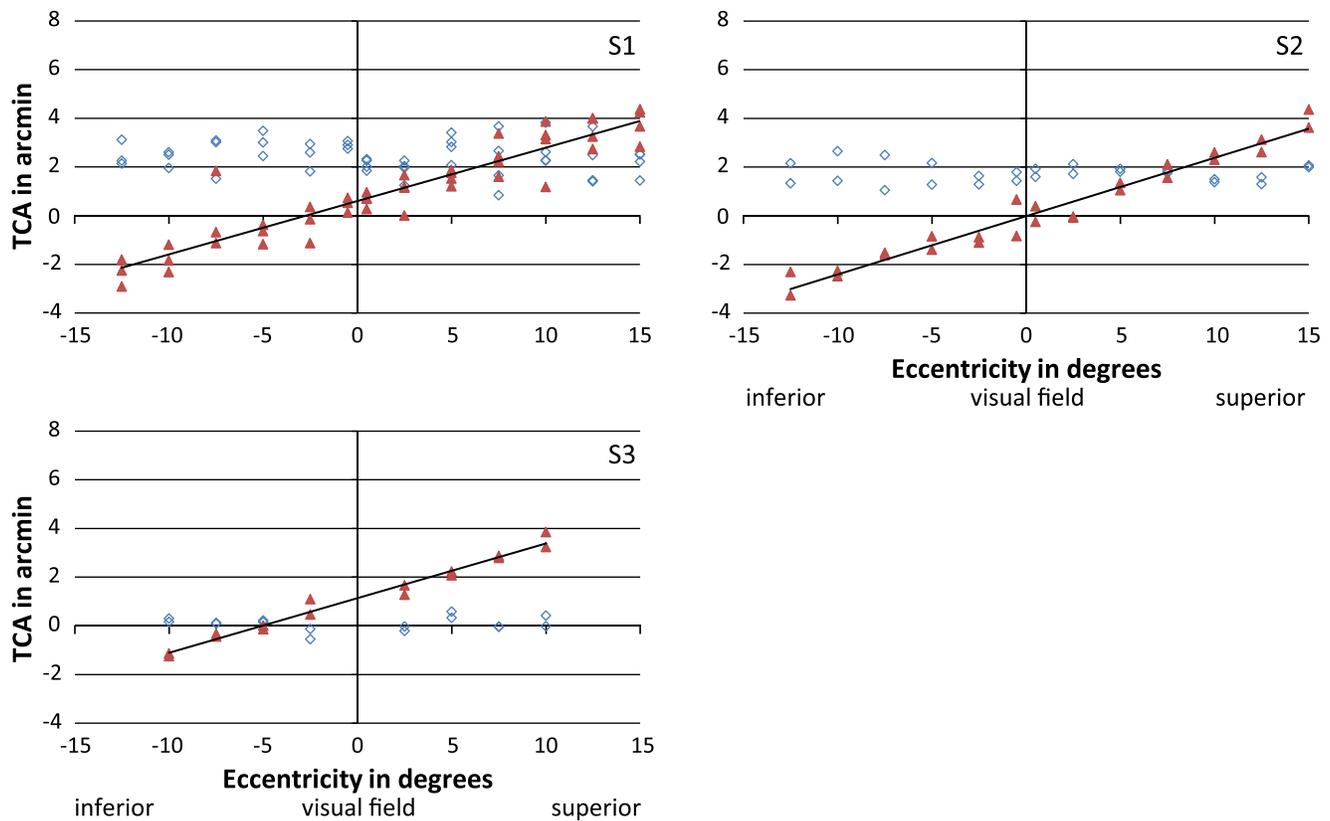
Figure 3. TCA in the vertical meridian for three subjects S1–S3. The blue hollow diamonds show the horizontal TCA, the red triangles the vertical TCA, and the line is a linear regression with the data given in Table 1. Note that the outlier for S1 in −7.5° is also included in the calculations. A positive sign of horizontal TCA means that the direction of TCA is the same as a base-in prism would cause (i.e., short wavelengths will end up at the retina more toward the nasal retina than the longer wavelengths). In the same manner a positive sign for vertical TCA corresponds with a base-up prism.

values are indeed visible in some of the graphs of Figures 2 and 3. For example, subject S3 shows a small mismatch between the absolute value of the horizontal TCA from the control measurement in Figure 3 compared with its value in Figure 2 at 0° eccentricity. Apart from the positioning of the subject's eye, it should be noted that the TCA was measured in a dilated pupil. It has been shown earlier that dilation can move the pupil center up to around 0.5 mm (Donnenfeld, 2004; Hoang et al., 2016; Walsh, 1988; Wilson, Campbell, & Simonet, 1992), which could potentially cause an additional offset in TCA of up to 2 arcmin compared with the natural pupil. Furthermore, the alignment of the pupil camera to the axis of the AOSLO in our experiment was made with an accuracy of around 1–2 pixels, corresponding to 0.05–0.10 mm in possible systematic off-set of the pupil. Using the formula mentioned already, such an off-set could in the worst case have given rise to a systematic error in the measured TCA of up to 0.2–0.4 arcmin. Naturally, both a systematic off-set and a random variation in pupil alignment will affect the actual magnitude of the measured TCA. However, the dependence on how

TCA changes with the off-axis viewing angle is not affected by such measurement errors.

To compare the results of this study with earlier studies of TCA, the magnitude of TCA and its change with eccentricity needs to be recalculated to other spectral ranges. For simplicity, we have assumed that TCA changes proportionally to the change in refractive index and used the same refractive index distribution as the Chromatic Eye by Thibos et al. $[n(\lambda) = 1.320535 +$

Subject	Horizontal meridian			Vertical meridian		
	Slope	Constant	R^2	Slope	Constant	R^2
S1	−0.22	2.5	0.95	0.22	0.6	0.87
S2	−0.15	2.3	0.73	0.24	0.0	0.96
S3	−0.26	1.8	0.93	0.22	1.1	0.98
S4	−0.13	1.9	0.81	-	-	-
Average	−0.19	2.1		0.23	0.6	
Std	0.06	0.3		0.01	0.6	

Table 1. TCA over the visual field as calculated from the regression lines in Figures 2 and 3 (TCA in arcmin = slope × field angle in degrees + constant).

Visual field	TCA (arcmin)			Cone spacing (arcmin)			mRGCf (arcmin)
	Mean	Min	Max	Mean	Min	Max	
Nasal 10° (hTCA)	4.0	3.2	4.8	2.24	2.05	2.53	4.59
Fovea (hTCA)	2.1	1.8	2.5	-	-	-	0.53
Temporal 10° (hTCA)	0.2	−0.8	0.8	2.25	1.97	2.73	4.35
Inferior 10° (vTCA)	−1.7	−2.4	−1.1	2.21	1.85	2.69	5.95
Fovea (vTCA)	0.6	0.0	1.1	-	-	-	0.53
Superior 10° (vTCA)	2.9	2.4	3.4	2.28	2.12	2.47	5.34

Table 2. TCA magnitude over the visual field for 543 to 842 nm and corresponding cone spacing in the retina (foveal cones could not be resolved). The first three data rows show the horizontal TCA (hTCA) over the horizontal visual field and the last three show the vertical TCA (vTCA) over the vertical visual field. The last column gives the midget ganglion cell receptive field sizes (mRGCf) for the same locations (Watson, 2014).

0.004685 / (λ - 0.214102)] (Thibos et al., 1992). Table 3 presents the same measured TCA over the horizontal field as Table 2, but recalculated for a visible wavelength range of 430–770 nm. Additionally, Table 3 also includes the results from five earlier studies on foveal TCA comprising data from 101 subjects (Marcos et al., 1999; Ogboso & Bedell, 1987; Rynders et al., 1995; Simonet & Campbell, 1990; Thibos et al., 1990). This foveal data is heavily weighted for the 85 subjects in the study by Rynders et al. (1995); if we only consider the data from the four other studies, the corresponding mean value would be 1.9 arcmin, with TCA ranging from −0.5 to 7.3 arcmin. The TCA from earlier studies at 10° off-axis in Table 3 is from the study by Ogboso & Bedell (1987). The last column shows a theoretical prediction of TCA. In his model, Thibos expected the change of TCA with eccentricity to be 0.28 arcmin/degree for the spectral range of 430 nm to 770 nm (Thibos, 1987). Recalculating our results on a slope in TCA of 0.21 arcmin/degree for the same spectrum would give 0.41 arcmin/degree. It can thereby be concluded that our objective measurements of TCA yields somewhat larger foveal TCA and faster rate of change than earlier reports. However, the current data is still within the earlier reported range of large individual variations in foveal TCA.

Implications of TCA for vision, imaging and vision testing

For vision, the TCA measured at 10° in the nasal visual field (7.8 arcmin when recalculated to a visual spectrum from 430 to 770 nm) is larger than the midget retinal ganglion cell receptive field size estimates (4.59 arcmin for ON mRGCs; Watson, 2014) and cone photoreceptor spacing (2.24 arcmin). Hence, the TCA blur can cover three to four cones (see Figure 4). We therefore conclude that the peripheral TCA can be visually significant. Even though the resolution acuity at that location is sampling limited with around 3-5 arcmin (Thibos, 1987; Wertheim, 1894), low contrast resolution as well as detection can be limited by the contrast reduction. Such a decrease in peripheral detection acuity due to TCA has indeed been observed in previous studies (Cheney, Thibos, & Bradley, 2015; Venkataraman, Winter, Rosén, & Lundström, 2016; Winter et al., 2015).

For retinal imaging and vision testing, TCA will manifest in different ways depending on the specific modality. In all cases, TCA will vary across the visual field, giving rise to orientation-dependent blur and magnification differences across wide-field images, and lateral displacements between wavelengths for small-field images. Furthermore, in cases where intra-pupil or

Visual field	TCA from this study			TCA from earlier studies			Theory
	Mean	Min	Max	Mean	Min	Max	
Nasal 10° (hTCA)	7.8	6.2	9.3	3.8	3.1	5.1	4.2
Fovea (hTCA)	4.1	3.5	4.9	0.3	−7.7	7.7	1.4
Temporal 10° (hTCA)	0.4	−1.6	1.6	3.1	0.8	4.9	−1.4

Table 3. TCA magnitude in minutes of arc over the horizontal visual field for the visual spectrum (430–770 nm). Columns two through four show the recalculated data from Table 2. Columns five through seven summarize the data from previous studies, all recalculated to 430–770 nm; the foveal data is the summary of the five studies by Ogboso and Bedell (1987), Thibos et al. (1990), Simonet & Campbell (1990), Rynders et al. (1995), and Marcos et al. (1999), whereas the 10° data is from the study by Ogboso and Bedell (1987). The last column gives the theoretical prediction by Thibos (1987).
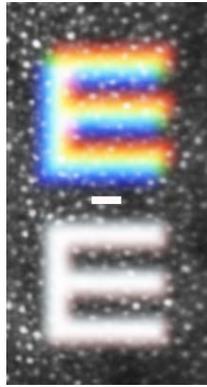
Figure 4. Simulation of the retinal image quality with (top) and without (bottom) ocular TCA at 10° eccentricity (LCA was corrected for in both cases). The bottom letter E has a stroke width of 4 arcmin and 1 arcmin of gaussian blur (best case scenario for the PSF). To simulate TCA in the upper image, blue (430 nm), green (555 nm), and red (770 nm) copies of the letter E are obliquely displaced by 7 arcmin, which corresponds with the TCA in the 10° superior-nasal visual field. The scale bar corresponds with 5 arcmin.

Maxwellian view illumination is used, the magnitude and sign of the induced TCA will be highly dependent on the position of the beam relative to the pupil center of the eye. Following are some specific examples of how TCA will have an impact:

- When imaging a small field at 10° eccentricity the lateral shifts between two wavelengths for a beam centered in the eye's pupil can be as high as 4.8 armin, or 23 μm (between 543 nm and 842 nm). In an application where the reflectance at two different wavelengths is compared with computed blood oxygenation levels, these lateral offsets can be two to four times larger than the capillary diameter.
- In some high resolution fluorescence imaging situations, a reflectance image is used to help guide the registration and integration of the weak fluorescence signal (Morgan, Dubra, Wolfe, Merigan, & Williams, 2009; Rossi et al., 2013). TCA resulting from large differences between the wavelength for reflectance and the wavelength for excitation can cause the fluorescence image to be displaced by more than the size of a cell body. Moreover, shifts in the alignment between the imaging beam and the eye's pupil will cause the TCA to vary over the course of the experiment. Incidentally, this is less of a concern for in vivo two-photon imaging where the reflectance and excitation wavelengths are both in the near infrared (Hunter et al., 2011; Sharma, Williams, Palczewska, Palczewski, & Hunter, 2016; Sharma et al., 2013; Sharma, Schwarz et et al., 2016).

- In a broad spectrum illumination setup, for example in fundus photography or in an optical coherence tomography system, the TCA would give rise to lateral blur in the image that varies across the imaged field.
- In AOSLO vision testing applications, near infrared light (e.g., 842 nm) is used to image and track the retina, and visible wavelengths are used to stimulate targeted retinal locations. The combined TCA of the system and the eye can be used to correct the placement of the stimulus (Harmening, Tuten, Roorda, & Sincich, 2014) or can be used to postcorrect the stimulus locations (Sincich, Zhang, Tiruveedhula, Horton, & Roorda, 2009). In any case, a failure to correct for TCA will give rise to offsets that are greater than the size of the targeted cell.

These few examples alone make it clear that the correction of TCA or an awareness of the implications of TCA is important for retinal imaging. The TCA measurements reported here relied on the use of a custom-built, high-resolution adaptive optics retinal imaging system. It is important to note, however, that a system with (a) careful pupil alignment, (b) a subjective measurement of foveal TCA (which can be made using Vernier alignment techniques), and (c) employing the fact that TCA increases linearly with eccentricity according to the values given in this work, can be used to achieve approximate individual estimates of the TCA in the ±15° visual field.

Acknowledgments

Commercial relationships: AR has two patents on technology related to the Adaptive Optics Scanning Laser Ophthalmoscope USPTO #7,118,216 and #6,890,076. These patents are assigned to both the University of Rochester and the University of Houston.

References

Atchison, D. A., & Smith, G. (2000). *Optics of the human eye*. Edinburgh, Scotland: Butterworth-Heinemann.

Atchison, D. A., & Smith, G. (2005). Chromatic dispersions of the ocular media of human eyes. *Journal of the Optical Society of America A*, *22*, 29–37.

Baskaran, K., Rosén, R., Lewis, P., Unsbo, P., & Gustafsson, J. (2012). Benefit of adaptive optics aberration correction at preferred retinal locus. *Optometry and Vision Science*, *89*, 1417–1423.

Cheney, F., Thibos, L., & Bradley, A. (2015). Effect of ocular transverse chromatic aberration on detection acuity for peripheral vision. *Ophthalmic and Physiological Optics*, *35*, 70–80.

Donnenfeld, E. (2004). The pupil is a moving target: Centration, repeatability, and registration. *Journal of Refractive Surgery*, *20*, S593–S596.

Dubra, A., Sulai, Y., Norris, J. L., Cooper, R. F., Dubis, A. M., Williams, D. R., & Carroll, J. (2011). Noninvasive imaging of the human rod photoreceptor mosaic using a confocal adaptive optics scanning ophthalmoscope. *Biomedical Optics Express*, *2*, 1864–76.

Duncan, J. L., Zhang, Y., Gandhi, J., Nakanishi, C., Othman, M., Branham, K. E. H., . . . Roorda, A. (2007). High-resolution imaging with adaptive optics in patients with inherited retinal degeneration. *Investigative Ophthalmology and Visual Science*, *48*, 3283–3291. [PubMed] [Article]

Grieve, K., Tiruveedhula, P., Zhang, Y., & Roorda, A. (2006). Multi-wavelength imaging with the adaptive optics scanning laser Ophthalmoscope. *Optics Express*, *14*, 12230–12242.

Gustafsson, J., & Unsbo, P. (2003). Eccentric correction for off-axis vision in central visual field loss. *Optometry and Vision Science*, *80*, 535–41.

Harmening, W. M., Tiruveedhula, P., Roorda, A., & Sincich, L. C. (2012). Measurement and correction of transverse chromatic offsets for multi-wave-length retinal microscopy in the living eye. *Biomedical Optics Express*, *3*, 2066–2077.

Harmening, W. M., Tuten, W. S., Roorda, A., & Sincich, L. C. (2014). Mapping the perceptual grain of the human retina. *The Journal of Neuroscience*, *34*, 5667–77.

Hoang, T. A., Macdonnell, J. E., Mangan, M. C., Monsour, C. S., Polwattage, B. L., Wilson, S. F., . . . Atchison, D. A. (2016). Time course of pupil center location after ocular drug application. *Optometry and Vision Science*, *93*, 594–599.

Holden, B., Sankaridurg, P., Smith, E., Aller, T., Jong, M., & He, M. (2014). Myopia, an underrated global challenge to vision: Where the current data takes us on myopia control. *Eye*, *28*, 142–146.

Hunter, J. J., Masella, B., Dubra, A., Sharma, R., Yin, L., Merigan, W. H., . . . Williams, D. R. (2011). Images of photoreceptors in living primate eyes using adaptive optics two-photon ophthalmoscopy. *Biomedical Optics Express*, *2*, 139–148.

Jaeken, B., Lundström, L., & Artal, P. (2011). Peripheral aberrations in the human eye for different wavelengths: Off-axis chromatic aberration. *Journal of the Optical Society of America A*, *28*, 1871–1879.

Lundström, L., Gustafsson, J., & Unsbo, P. (2007). Vision evaluation of eccentric refractive correction. *Optometry and Vision Science*, *84*, 1046–1052.

Marcos, S., Burns, S. A., Moreno-Barriusop, E., & Navarro, R. (1999). A new approach to the study of ocular chromatic aberrations. *Vision Research*, *39*, 4309–4323.

Morgan, J. I. W., Dubra, A., Wolfe, R., Merigan, W. H., & Williams, D. R. (2009). In vivo autofluorescence imaging of the human and macaque retinal pigment epithelial cell mosaic. *Investigative Ophthalmology & Visual Science*, *50*, 1350–1359. [PubMed] [Article]

Ogboso, Y. U., & Bedell, H. E. (1987). Magnitude of lateral chromatic aberration across the retina of the human eye. *Journal of the Optical Society of America A*, *4*, 1666–1672.

Privitera, C. M., Sabesan, R., Winter, S., Tiruveedhula, P., & Roorda, A. (2016). Eye-tracking technology for real-time monitoring of transverse chromatic aberration. *Optics Letters*, *41*, 1728–1731.

Roorda, A., Romero-Borja, F., Donnelly, W., Queener, H., Hebert, T., & Campbell, M. C. W. (2002). Adaptive optics scanning laser ophthalmoscopy. *Optics Express*, *10*, 405–412.

Rossi, E. A., Rangel-Fonseca, P., Parkins, K., Fischer, W., Latchney, L. R., Folwell, M. A., . . . Chung, M.

Winter et al.

M. (2013). In vivo imaging of retinal pigment epithelium cells in age related macular degeneration. *Biomedical Optics Express*, 4, 2527–2539.

Rynders, M., Lidkea, B., Chisholm, W., & Thibos, L. N. (1995). Statistical distribution of foveal transverse chromatic aberration, pupil centration, and angle psi in a population of young adult eyes. *Journal of the Optical Society of America A*, 12, 2348–2357.

Rynders, M., Navarro, R., & Losada, M. A. (1998). Objective measurement of the off-axis longitudinal chromatic aberration in the human eye. *Vision Research*, 38, 513–522.

Sharma, R., Schwarz, C., Williams, D. R., Palczewska, G., Palczewski, K., & Hunter, J. J. (2016). In vivo two-photon fluorescence kinetics of primate rods and cones. *Investigative Ophthalmology & Visual Science*, 57, 647–657. [PubMed] [Article]

Sharma, R., Williams, D. R., Palczewska, G., Palczewski, K., & Hunter, J. J. (2016). Two-photon autofluorescence imaging reveals cellular structures throughout the retina of the living primate eye. *Investigative Ophthalmology & Visual Science*, 57, 632–646. [PubMed] [Article]

Sharma, R., Yin, L., Geng, Y., Merigan, W. H., Palczewska, G., Palczewski, K., . . . Hunter, J. J. (2013). In vivo two-photon imaging of the mouse retina. *Biomedical Optics Express*, 4, 1285–1293.

Simonet, P., & Campbell, M. C. W. (1990). The optical transverse chromatic aberration on the fovea of the human eye. *Vision Research*, 30, 187–206.

Sincich, L. C., Zhang, Y., Tiruveedhula, P., Horton, J. C., & Roorda, A. (2009). Resolving single cone inputs to visual receptive fields. *Nature Neuroscience*, 12, 967–969.

Thibos, L. N. (1987). Calculation of the influence of lateral chromatic aberration on image quality across the visual field. *Journal of the Optical Society of America A*, 4, 1673–1680.

Thibos, L. N., Bradley, A., Still, D. L., Zhang, X., & Howarth, P. A. (1990). Theory and measurement of ocular chromatic aberration. *Vision Research*, 30, 33–49.

Thibos, L. N., Ye, M., Zhang, X., & Bradley, A. (1992). The chromatic eye: A new reduced-eye model of ocular chromatic aberration in humans. *Applied Optics*, 3594–3600.

Venkataraman, A. P., Winter, S., Rosén, R., & Lundström, L. (2016). Choice of grating orientation for evaluation of peripheral vision. *Optometry & Vision Science*, 93, 567–574.

Vinas, M., Dorronsoro, C., Cortes, D., Pascual, D., & Marcos, S. (2015). Longitudinal chromatic aberration of the human eye in the visible and near infrared from wavefront sensing, double-pass and psychophysics. *Biomedical Optics Express*, 23, 513–522.

Walsh, G. (1988). The effect of mydriasis on the pupillary centration of the human eye. *Ophthalmic and Physiological Optics*, 8, 178–82.

Watson, A. B. (2014). A formula for human retinal ganglion cell receptive field density as a function of visual field location. *Journal of Vision*, 14(7):15, 1–17, doi:10.1167/14.7.15. [PubMed] [Article]

Wertheim, T. (1894). Über die indirekte Sehschärfe. *Zeitschrift für Psychologie und Physiologie der Sinnesorgane*, 7, 172–187.

Wilson, M. A., Campbell, M. C. W., & Simonet, P. (1992). The Julius F. Neumueller Award in Optics, 1989: Change of pupil centration with change of illumination and pupil size. *Optometry and Vision Science*, 69, 129–136.

Winter, S., Fathi, M. T., Venkataraman, A. P., Rosén, R., Seidemann, A., Esser, G., . . . Unsbo, P. (2015). Effect of induced transverse chromatic aberration on peripheral vision. *Journal of the Optical Society of America A*, 32, 1764–1771.